

53BP1 cooperation with the REV7-Shieldin complex underpins DNA structure-specific NHEJ (86 characters, inc. spaces; limit 90)

Hind Ghezraoui^{1,6}, Catarina Oliveira^{1,6}, Jordan R. Becker¹, Kirstin Bilham¹, Daniela Moralli², Consuelo Anzilotti³, Roman Fischer⁵, Mukta Deobagkar-Lele³, Maria Sanchiz-Calvo¹, Elena Fueyo-Marcos¹, Sarah Bonham⁵, Benedikt M. Kessler⁵, Sven Rottenberg⁴, Richard J. Cornall³, Catherine M. Green², J. Ross Chapman^{1*}

¹Genome Integrity Laboratory, Wellcome Centre for Human Genetics, University of Oxford, OX3 7BN, UK.

²Chromosome Dynamics, Wellcome Centre for Human Genetics, University of Oxford, OX3 7BN, UK.

³MRC Human Immunology Unit, Weatherall Institute for Molecular Medicine, Nuffield Department of Medicine, University of Oxford, Oxford, OX3 9DS, UK.

⁴Institute of Animal Pathology, Vetsuisse Faculty, University of Bern, Bern, Switzerland

⁵Target Discovery Institute, Nuffield Department of Medicine, University of Oxford, Roosevelt Drive, Oxford OX3 7FZ, UK.

⁶Equal contributing authors

*Correspondence: rchapman@well.ox.ac.uk

Summary (202 words)

53BP1 governs a specialised, context-specific branch of the classical non-homologous end joining (NHEJ) DNA double-strand break (DSB) repair pathway. *53bp1*^{-/-} mice are immunodeficient owing to a complete loss of immunoglobulin (Ig) class-switch recombination (CSR)^{1,2}, and reduced long-range V(D)J recombination fidelity³. The 53BP1-dependent pathway is additionally responsible for pathological joining events at dysfunctional telomeres⁴, and its unrestricted activity in *BRCA1*-deficient cellular and tumour models causes genomic instability and oncogenesis⁵⁻⁷. Cells lacking core NHEJ proteins are profoundly radiosensitive⁸, unlike 53BP1-deficient cells^{9,10}, suggesting that 53BP1 and its co-factors act on specific DNA substrates. Here, we show that 53BP1 cooperates with its downstream effector protein REV7 to promote NHEJ during CSR, yet REV7 is not required for 53BP1-dependent V(D)J recombination. We identify Shieldin, a four subunit putative single-stranded DNA-binding complex comprising REV7, c20orf196 (SHLD1), FAM35A (SHLD2), and FLJ26957 (SHLD3) as the factor that explains this specificity. Shieldin is essential for REV7-dependent DNA end-protection and NHEJ during CSR, and supports toxic NHEJ in *BRCA1*-deficient cells, yet is dispensable for REV7-

dependent interstrand cross-link (ICL) repair. The 53BP1 pathway therefore comprises distinct DSB repair activities within chromatin and single-stranded DNA (ssDNA) compartments, which explains both the immunological differences between *53bp1*- and *Rev7*- deficient mice and the pathway's context specificity.

Main Text – 1964 words

53BP1-dependent NHEJ requires the participation of several downstream factors^{9,11,12} including REV7, a non-catalytic subunit of the translesion synthesis (TLS) DNA polymerase Zeta (Pol-ζ). REV7 mediates genotoxic NHEJ events in *Brca1*-deficient mouse mammary tumour cells, and prevents end-resection at CSR-associated DSBs¹³. We generated a conditional *Rev7* knockout mouse (*Rev7^{F/F}*) in a C57BL/6 background, after germline *Rev7*-deletion resulted in embryonic lethality (Extended Data Table 1). *Rev7^{F/F}* mice possessing the B cell *Mb1-cre* deleter allele¹⁴ showed *Rev7* deletion at the start of the B cell-lineage (Extended Data Fig. 1a), and normal B cell numbers with undetectable REV7 protein (Extended Data Fig. 1b). *Rev7^{F/F} Mb1^{+Cre}* mice expressed normal serum IgM but reduced titres of IgA and IgG, suggestive of CSR failure (Fig. 1a). Defective *in vivo* CSR was confirmed in immunisation experiments in which serum concentrations of antigen-specific IgG1 in *Rev7^{F/F} Mb1^{+Cre}* mice were ~10-fold lower than in control *Rev7^{+/+} Mb1^{+Cre}* mice, while IgM responses were comparable between groups (Fig. 1b). Likewise, REV7-deletion severely compromised (by up to 90%) the production of class switched B splenocytes upon stimulation in culture (Fig. 1c and Extended Data Fig. 1c), without impacting cell proliferation (Fig. 1d). Equivalent CSR frequencies in *Rev7^{F/F} Mb1^{+Cre}*, *53bp1^{-/-} Mb1^{+Cre}*, and *53bp1^{-/-} Rev7^{F/F} Mb1^{+Cre}* double knockout cells furthermore confirmed REV7-53BP1 cooperation is essential for CSR (Fig. 1e).

However, stark differences in the absolute numbers of B lineage cells were detected between *Rev7^{F/F} Mb1^{+Cre}* and *53bp1^{-/-} Mb1^{+Cre}* mice (Fig. 1f). While *53bp1*-deficient mice showed 50% and 29% reductions in B220-positive B lymphocytes in the bone marrow (BM) and spleen, respectively, these abnormalities were absent from *Rev7^{F/F} Mb1^{+Cre}* animals (Fig. 1f), leading us to question whether 53BP1-dependent DNA repair activities during B cell development require REV7. Detailed BM analysis showed that B lymphocytes of *53bp1^{-/-} Mb1^{+Cre}* mice became progressively depleted, with ~70% losses in total lymphocytes by the late small pre-B and immature B cell stages (Hardy fractions D and E, respectively; Fig. 1g and Extended Data Fig. 2a). Losses were accompanied by increased apoptosis in BM and follicular (Fo) splenic B cell fractions (Extended Data Fig. 2b-c). In contrast, *Rev7^{F/F} Mb1^{+Cre}* mice showed normal B cell counts and apoptotic indices (Fig. 1g and Extended Data Fig. 2a-c), despite the complete absence of REV7 protein in B220⁺ CD43⁺ pro-B progenitors (Extended data Fig. 2d). To exclude the possibility that developmental defects in *Rev7^{F/F} Mb1^{+Cre}* mice could be masked by compensatory changes, we generated mixed BM chimeric mice. Equal mixes of CD45.1 WT and CD45.2 *Rev7^{F/F} Mb1^{+Cre}*, or CD45.1 WT and CD45.2 *53bp1^{-/-} Mb1^{+Cre}* whole BM cells were

77 injected intravenously into lethally irradiated CD45.1 WT recipient mice (Extended data Fig. 2e).
 78 8 weeks after BM transfer, the reconstitution of pro, pre, immature and mature BM B cells
 79 derived from CD45.2 *Rev7^{F/F} Mb1^{+/-Cre}* did not differ from WT CD45.1, similar to that in control
 80 recipient mice (Extended data Fig. 2e). However, BM B cells derived from CD45.2 *53bp1^{-/-}*
 81 *Mb1^{+/-Cre}* mice only reconstituted ~30% of pro-B cell fractions, and were further outcompeted by
 82 WT CD45.1 BM B cells at later stages, where they only made up ~15% of total immature and
 83 mature fractions (Extended data Fig. 2e). These findings confirmed that B cell development is
 84 normal in the absence of REV7, suggesting 53BP1-dependent V(D)J recombination, which is
 85 essential for this process, does not require REV7.

86 To directly test whether 53BP1-dependent NHEJ during V(D)J recombination and CSR
 87 could be distinguished at the level of REV7 involvement, we monitored the stability of the *Igh* and
 88 *Ig* lambda light chain (*Igl*) loci in stimulated B splenocytes from *Rev7^{F/F} Mb1^{+/-Cre}*, *53bp1^{-/-}*, and
 89 control (*Mb1^{+/-Cre}*) mice. Upon stimulation with anti-CD40 plus IL-4 *in vitro*, NHEJ-deficient splenic
 90 B cells accumulate *Igl* breaks due to abortive RAG1/2-dependent secondary V-J recombination
 91 events and *Igh* breaks associated with CSR¹⁵. Chromosome breakage at *Igh* and *Igl* was
 92 monitored by 4-colour FISH (Fluorescence *In Situ* Hybridization) on metaphase spreads using
 93 probes positioned centromeric and telomeric to these loci¹⁵. Metaphases were classed as
 94 abnormal if either locus had bi-allelic centromeric BAC signals, with one allele lacking an
 95 adjacent signal from the telomeric BAC (Fig. 1h). As expected, *53bp1^{-/-}* B cells had high levels of
 96 chromosomal abnormalities at both the *Igh* and *Igl* loci, unlike control cells where locus breakage
 97 was rare (Fig. 1i). 3 out of 4 *Rev7^{F/F} Mb1^{+/-Cre}* mice exhibited breakage frequencies at the *Igh*
 98 locus equivalent to *53bp1^{-/-}* mice. In contrast, *Igl* abnormalities in *Rev7^{F/F} Mb1^{+/-Cre}* cells occurred
 99 at near control frequencies, consistent with a selective requirement for 53BP1, but not REV7, in
 100 V(D)J recombination.

101 To determine REV7's function in CSR, we deleted *Rev7* in CH12-F3, a mouse B
 102 lymphoma cell-line that undergoes efficient switching from IgM to IgA upon stimulation *in vitro*.
 103 ~10-fold CSR defects in *Rev7^{-/-}* CH12-F3 were suppressed by reconstitution of REV7 expression
 104 (Fig. 2a), and >20 REV7 single/combinatorial point mutants were screened for their ability to
 105 restore CSR (Fig. 2b and Extended Data Fig. 3a,b). Mutations were selected which disrupt
 106 protein interactions^{16,17}, post-translational modifications, or a Destruction-box degron¹⁸, and
 107 structure-led conservation analysis guided the generation of mutants within putative protein-
 108 interaction surfaces (summarised in Extended Data Table 2). Stable CSR-defective REV7
 109 mutants were re-tested for their ability to support CSR to IgG1 upon complementation in
 110 stimulated B cells from *Rev7^{F/F} Mb1^{+/-Cre}* mice (Fig. 2c, d). Two mutants, REV7^{Y63A} and
 111 REV7^{K129A}, failed to rescue CSR to levels above that of control-complemented cells in both
 112 screens. The capacity of these mutants to prevent the hyper-resection of *Igh* switch (S) region
 113 DSBs, a central function of the 53BP1-RIF1-REV7 axis during CSR^{9,11,13,19}, was therefore
 114 assessed by RPA-ssDNA chromatin immunoprecipitation (ChIP) across *Igh* and control loci. As

expected¹³, DSB-associated donor (*S μ*) and acceptor (*S α*) *S* loci, but not non-targeted *Igh* (*S γ 1*) or control (*Rpp30*) loci, exhibited aberrant RPA-ssDNA enrichments in *Rev7*^{-/-} cells (Extended data Fig. 3c). RPA-enrichments were suppressed in cell-lines expressing WT REV7, but not the REV7^{Y63A} or REV7^{K129A} mutants, confirming these mutations compromise resection inhibition (Extended data Fig. 3c).

REV7 Tyr-63 is one of two evolutionarily-conserved residues that mediate interactions between the C-terminal 'safety-belt' domain and two conserved REV7-binding motifs in REV3L (RBM₁ and RBM₂; consensus PxxxpPSR)^{17,20}, each of which is essential for REV3L-dependent resistance to ICL damage²⁰. Alanine-substitutions at Tyr-63 or Trp-171 in REV7 blocked REV3L RBM₁ yeast-2-hybrid (Y2H) interactions (Extended data Fig. 4a). As expected²¹, *Rev7*^{-/-} cells were sensitive to the ICL inducer MMC, first accumulating in G2/M, then progressing into cell death marked by an accumulation of sub-G1 events and profound chromosomal instability (Extended data Fig. 4b-d). These defects were completely suppressed by complementation with WT REV7, but not REV7^{Y63A} nor REV7^{W171A} mutants, nor the REV1 binding mutants REV7^{L186A} or REV7^{Y202A} (Extended data Fig. 4b, e). In contrast, the CSR-deficient REV7^{K129A} mutant completely restored WT responses to MMC, in agreement with its unperturbed interaction with REV3L (Extended Data Fig. 4e, a). This separation of function between REV7 ICL repair and NHEJ activities implicates distinct REV7 complexes in NHEJ.

We therefore immunopurified control and Flag-HA-REV7 complexes from lysates of stably-complemented *Rev7*^{-/-} CH12-F3, and analysed these by LC-MS/MS. Aside from the known interactors REV3L and GTF2I²², three uncharacterized proteins were highly enriched with REV7 (Fig. 3a, Table 1). Each of these genes, FAM35A, c20orf196 and FLJ26957/CTC-5342.2 (renamed SHLD1, SHLD2 and SHLD3, respectively), was cloned and screened for interaction with WT and mutant REV7 by Y2H. In this assay, only SHLD3 showed direct interaction with REV7, and this was abolished by REV7^{Y63A}, yet unaffected by REV7^{W171A} (Fig. 3b and Table 1), correlating perfectly with the requirement for Tyr-63 but not Trp-171 in NHEJ. SHLD3 comprises two N-terminal REV3L-like RBM motifs, and predicted structural folds that resemble the mRNA cap-binding domain of the translational elongation initiation factor EIF4E (Fig. 3c; folds recognized by Phyre2²³). REV7-SHLD3 interactions rely predominantly on Pro-53 and Pro-58 in RBM₂ (Fig. 3c), a motif resembling RBM₁ in REV3L (Extended Data Figure 5a).

The CSR defects exhibited by REV7^{K129A} could not be explained by failure to interact with SHLD3 (Fig. 3b). Lys-129 is a highly conserved residue on an uncharacterized structural surface, selected upon analysis of the REV7 crystal structure¹⁶ (Extended Data Figure 5b). A mutant harboring a conservative arginine substitution of Lys-129 completely restored WT CSR frequencies (Fig. 2b and Extended Data Fig. 3b), eliminating consideration of post-translational modification. Thus, Flag-HA-Rev7^{K129A} and WT Flag-HA-REV7 complex compositions were compared by LC-MS/MS and LFQ. Consistent with Y2H data, Flag-HA-Rev7^{K129A} complexes

retained equivalent levels of REV3L and SHLD3, yet were devoid of SHLD1-SHLD2 (Fig. 3d and Table 1), implicating these factors in NHEJ.

Isogenic knockout CH12-F3 clones were therefore generated for *Shld1-3*. No changes in REV7 or 53BP1 expression were identified in these knockout cell-lines (Extended Data Fig. 6a), suggesting a direct role for (SHLD1-3)-REV7 complexes in NHEJ. Normal proliferation, but diminished CSR, was detected in all clones (Fig. 4a-b, Extended Data Fig. 6b). CSR was restored in *Shld3*^{-/-} and *Shld2*^{-/-} cells by integration of *Shld3* and *Shld2* transgenes, respectively (Fig. 4c and Extended Data Fig. 6c), with mutant *Shld3* transgenes revealing RBM₁₋₂ support CSR redundantly (Fig 4c. and Extended data Fig. 6d). *Shld3*-deletion did not augment CSR defects in *Rev7*^{-/-} CH12-F3 (Extended Data Fig. 6e), confirming epistasis between *Shld3* and *Rev7* in NHEJ. These data indicate REV7 forms the linchpin in a 4-subunit protein complex, whose integrity is essential for 53BP1-dependent CSR: REV7's C-terminal safety-belt mediates interaction with SHLD3; while residues centered around Lys-129 mediate binding to SHLD1-SHLD2 heterodimers. Structural modeling of SHLD2 revealed a triple-tandem OB-fold architecture with structural homology to the core ssDNA-binding OB-folds₂₋₄ in fungal RPA70²⁴ (Extended Data Fig. 5c-d). We, and others (Ref Noordermeer), have thus named this putative ssDNA-binding complex 'Shieldin', and its subunits SHLD1, SHLD2, and SHLD3, in analogy to the telomere end-capping complex Shelterin, whose ssDNA and double-stranded DNA (dsDNA) binding proteins cooperate in chromosome end protection²⁵.

RPA-ssDNA ChIP experiments confirmed Shieldin's contribution to DNA-end protection: RPA-ssDNA complexes were un-detectable at donor (*Sμ*) and acceptor (*Sα*) loci in stimulated cultures of WT and SHLD3-complemented *Shld3*^{-/-} CH12-F3, yet highly enriched in *Rev7*^{-/-}, *Shld2*^{-/-}, and *Shld3*^{-/-} cells (Fig. 4d and Extended Data Fig. 6f-g). Thus, REV7-Shieldin inhibits DSB resection during NHEJ. However, *Shld3*^{-/-} cell lines were indistinguishable from control upon MMC treatment, consistent with REV7 separation-of-function in ICL repair and NHEJ (Extended Data Fig. 6h).

We next investigated Shieldin's contribution to 53BP1-dependent toxic NHEJ in *BRCA1*-deficient cells. CRISPR-Cas9-mediated mutagenesis of *Shld3* in the *Brca1*^{-/-} *p53*^{-/-} mouse mammary tumour cell-line KB1P-G3¹³ was strongly selected for in the presence of the PARPi olaparib (Extended Data Fig. 6i). Moreover, PARPi-resistance in *Shld3*^{-/-} KBP1-G3 cells was equivalent to *Rev7*^{-/-} KBP1-G3 controls (Fig. 4e-f). There was neither selection for mutagenesis of *Shld3* or *Rev7* loci in olaparib-treated *53bp1*^{-/-} KB1P-G3, nor increased resistance in *Shld3*^{-/-} *53bp1*^{-/-} cells (Fig. 4f and Extended Data Fig. 6j-k). Similar reductions in olaparib-induced radial chromosomes in both *Shld3*^{-/-} and *53bp1*^{-/-} KB1P-G3 lines confirmed toxic NHEJ in *BRCA1*-deficient cells is Shieldin-dependent (Fig. 4g). Shieldin disruption therefore provides a possible route to PARPi resistance in cancer.

This study reveals a requirement for a putative ssDNA-binding protein complex, Shieldin, in the 53BP1 pathway, indicating that multiple DNA binding activities cooperate during DNA

structure-specific NHEJ (Fig. 4h). Coupling of 53BP1-dependent anti-resection activities within chromatin, to Shieldin-dependent stabilization of ssDNA-tailed ends, may permit the conversion of ssDNA-tailed substrates such as those generated during CSR, into DSBs amenable to NHEJ. This segregation of distinct, yet cooperative activities at DSB sites can explain the developmental differences between 53BP1- and REV7- deficient lymphocytes: The ssDNA-tails of AID-dependent DSBs induced during CSR require these specialized activities to orchestrate their joining by NHEJ²⁶, whereas the absence of ssDNA at RAG-induced DSBs produced during V(D)J recombination could preclude the need for Shieldin. ssDNA-tailed DSBs additionally exist at uncapped telomeres, and potentially at collapsed replication forks, and thus a requirement for Shieldin during the repair of these structures can explain the physiological and pathophysiological specificities of the 53BP1 system.

Protein ID	Flag-HA-REV7 (wild-type)		LFQ; avg log2 FT (WT/cntl, n=2)	LFQ; avg log2 FT (K129A/WT, n=2)	Y2H interaction with REV7
	# unique peptides	Coverage (%)			
REV7 (MAD2L2)	9	42	5.1	-0.5	NA
c20orf196 (SHLD1)	5	34	5.7	-7.8	-
FAM35A (SHLD2)	15	26	6.9	-6.6	-
FLJ26957 (SHLD3)	8	27	4.3	-1.01	+
REV3L	8	3	1.8	0.02	+
GTF2I	10	12	2.7	0.95	ND

(Table 1. – see below for legends)

Acknowledgements -141 words

We thank members of the Chapman, Green, Cornall and Rottenberg laboratories for discussions, T. Humphrey for comments on the manuscript. We thank D. Adams for the *Rev7^{tm1a}* mouse strain, S. Boulton for *53bp1^{-/-}* mice, J. Grimes and R. Nolan for assistance with protein modeling and statistics, and B. Davies, M. Barazas, B. Reina-San-Martin, Bart Deplancke, L. Vasilieva, A. Nussenzweig and E. Callen-Moreau for reagents and advice. This project was funded by Medical Research Council (MRC) Grant (MR/M009971/1) and Cancer Research UK Career Development Fellowship (C52690/A19270) awarded to J.R.C.. C.A. and M.D.-L. are funded by the MRC, R.J.C. is a Principal Investigator of the MRC Human Immunology Unit. R.F. and B.M.K. are supported by the Kennedy Trust and the John Fell Fund. M.S.-C. and E.M.-F. were supported by ERASMUS+ fellowships. The Wellcome Centre for Human Genetics is supported by Wellcome grant (090532/Z/09/Z).

Author contributions – 119 words

H.G. and C.O. designed and performed the majority of the experiments and analysed the data with assistance from K.B., C.A., M.D-L., M.S.-C., E.F.-M. and R.J.C.. J.R.B. designed and performed the KB1P-G3 experiments and analysed the data. K.B. performed and analysed the immunisation and ELISA experiments, established the mixed chimeras, and coordinated animal experiments. D.M. and C.M.G. performed and analysed all FISH and metaphase chromosome experiments. R.F. ran and analysed the LC-MS/MS experiments with assistance from S.B. and supervision from B.M.K.. This study was initiated in collaboration with S.R.. J.R.C. conceived and supervised the study, performed experiments, analysed the data, prepared the figures and wrote the manuscript with editorial contributions from all authors. The authors declare no competing financial interests.

Materials and correspondence: rchapman@well.ox.ac.uk

Data availability statement: The mass spectrometry proteomics data have been deposited to the ProteomeXchange Consortium via the PRIDE partner repository with the dataset identifier PXD009650 and 10.6019/PXD009650.

References

1. Ward, I. M. *et al.* 53BP1 is required for class switch recombination. *J Cell Biol* **165**, 459–464 (2004).
2. Manis, J. P. *et al.* 53BP1 links DNA damage-response pathways to immunoglobulin heavy chain class-switch recombination. *Nat Immunol* **5**, 481–487 (2004).
3. Difilippantonio, S. *et al.* 53BP1 facilitates long-range DNA end-joining during V(D)J recombination. *Nature* **456**, 529–533 (2008).
4. Dimitrova, N., Chen, Y.-C. M., Spector, D. L. & De Lange, T. 53BP1 promotes non-homologous end joining of telomeres by increasing chromatin mobility. *Nature* **456**, 524–528 (2008).
5. Cao, L. *et al.* A selective requirement for 53BP1 in the biological response to genomic instability induced by Brca1 deficiency. *Mol Cell* **35**, 534–541 (2009).
6. Bunting, S. F. *et al.* 53BP1 inhibits homologous recombination in Brca1-deficient cells by blocking resection of DNA breaks. *CELL* **141**, 243–254 (2010).
7. Bouwman, P. *et al.* 53BP1 loss rescues BRCA1 deficiency and is associated with triple-negative and BRCA-mutated breast cancers. *Nat Struct Mol Biol* **17**, 688–695 (2010).
8. Lieber, M. R., Ma, Y., Pannicke, U. & Schwarz, K. Mechanism and regulation of human non-homologous DNA end-joining. *Nat Rev Mol Cell Biol* **4**, 712–720 (2003).
9. Chapman, J. R. *et al.* RIF1 is essential for 53BP1-dependent nonhomologous end joining and suppression of DNA double-strand break resection. *Mol Cell* **49**, 858–871 (2013).

- 257 10. Cuella-Martin, R. *et al.* 53BP1 Integrates DNA Repair and p53-Dependent Cell Fate
258 Decisions via Distinct Mechanisms. *Mol Cell* **64**, 51–64 (2016).
- 259 11. Di Virgilio, M. *et al.* Rif1 Prevents Resection of DNA Breaks and Promotes
260 Immunoglobulin Class Switching. *Science* **339**, 711–715 (2013).
- 261 12. Escribano-Diaz, C. *et al.* A cell cycle-dependent regulatory circuit composed of 53BP1-
262 RIF1 and BRCA1-CtIP controls DNA repair pathway choice. *Mol Cell* **49**, 872–883 (2013).
- 263 13. Xu, G. *et al.* REV7 counteracts DNA double-strand break resection and affects PARP
264 inhibition. *Nature* **521**, 541–544 (2015).
- 265 14. Hobeika, E. *et al.* Testing gene function early in the B cell lineage in mb1-cre mice. *Proc*
266 *Natl Acad Sci USA* **103**, 13789–13794 (2006).
- 267 15. Wang, J. H. *et al.* Mechanisms promoting translocations in editing and switching
268 peripheral B cells. *Nature* **460**, 231–236 (2009).
- 269 16. Wojtaszek, J. *et al.* Structural basis of Rev1-mediated assembly of a quaternary
270 vertebrate translesion polymerase complex consisting of Rev1, heterodimeric polymerase
271 (Pol) ζ , and Pol κ . *Journal of Biological Chemistry* **287**, 33836–33846 (2012).
- 272 17. Hara, K. *et al.* Crystal structure of human REV7 in complex with a human REV3 fragment
273 and structural implication of the interaction between DNA polymerase zeta and REV1.
274 *Journal of Biological Chemistry* **285**, 12299–12307 (2010).
- 275 18. Listovsky, T. & Sale, J. E. Sequestration of CDH1 by MAD2L2 prevents premature APC/C
276 activation prior to anaphase onset. *J Cell Biol* **203**, 87–100 (2013).
- 277 19. Hakim, O. *et al.* DNA damage defines sites of recurrent chromosomal translocations in B
278 lymphocytes. *Nature* **484**, 69–74 (2012).
- 279 20. Tomida, J. *et al.* REV7 is essential for DNA damage tolerance via two REV3L binding
280 sites in mammalian DNA polymerase ζ . *Nucleic Acids Res* **43**, 1000–1011 (2015).
- 281 21. Bluteau, D. *et al.* Biallelic inactivation of REV7 is associated with Fanconi anemia. *J. Clin.*
282 *Invest.* **126**, 3580–3584 (2016).
- 283 22. Fattah, F. J. *et al.* The transcription factor TFII-I promotes DNA translesion synthesis and
284 genomic stability. *PLoS Genet* **10**, e1004419 (2014).
- 285 23. Kelley, L. A., Mezulis, S., Yates, C. M., Wass, M. N. & Sternberg, M. J. E. The Phyre2
286 web portal for protein modeling, prediction and analysis. *Nat Protoc* **10**, 845–858 (2015).
- 287 24. Fan, J. & Pavletich, N. P. Structure and conformational change of a replication protein A
288 heterotrimer bound to ssDNA. *Genes Dev* **26**, 2337–2347 (2012).
- 289 25. Palm, W. & De Lange, T. How shelterin protects mammalian telomeres. *Annu Rev Genet*
290 **42**, 301–334 (2008).
- 291 26. Stavnezer, J. & Schrader, C. E. IgH chain class switch recombination: mechanism and
292 regulation. *The Journal of Immunology* **193**, 5370–5378 (2014).

293 27. Hardy, R. R., Carmack, C. E., Shinton, S. A., Kemp, J. D. & Hayakawa, K. Resolution and
294 characterization of pro-B and pre-pro-B cell stages in normal mouse bone marrow. *J Exp*
295 *Med* **173**, 1213–1225 (1991).
296
297

Figure Legends – 837 words

Figure 1. REV7 and 53BP1 cooperate during CSR, yet are functionally uncoupled in V(D)J recombination.

(A) Serum immunoglobulin in *Rev7^{+/+}Mb1^{+/-Cre}* and *Rev7^{F/F}Mb1^{+/-Cre}* mouse cohorts; *n*=11 mice per genotype; *p* values, unpaired two-tailed t-test. Mean ± 95% CI.

(B) NP-specific serum IgM (left) and IgG (right) at indicated times after NP-CGG immunisation; Representative data, *n*=2 independent experiments, each with 4 mice. Mean ± 95% CI.

(C) Cell trace violet (CTV)-labelled splenic B cells were stimulated as indicated and stained for surface IgG1 or IgE on day 4. Representative data, *n*>6 mice.

(D) CTV dilution in purified B cells cultured in the presence of LPS and IL-4 for 96 hours. Representative data, *n*>6 mice.

(E) Splenic B cells cultured with the indicated stimuli (96 h) and stained for surface IgG1, IgE, IgG2, IgG3. *n*=4 mice per genotype. 100% CSR, mean Ig isotype switch frequency of 2 control animals in each experiment. *p* values, two-way ANOVA with Tukey's correction. Mean ± 95% CI.

(F) Absolute numbers of B220+ B cells in the BM (1 femur plus 1 tibia) and spleen. *n*=9 mice per genotype, except *Rev7^{+/+}Mb1^{+/-Cre}* (*n*=8). *p* values, unpaired two-tailed t-test, Mean ± 95% CI.

(G) Absolute numbers of B cell precursors (Hardy²⁷ fractions A, B220+CD43+BP-1-CD24-; B, B220+CD43+BP-1-CD24+; C, B220+CD43+BP-1+CD24+; D, B220+CD43-IgM-IgD-; E, B220+CD43-IgM+IgD-; and F, B220+CD43-IgM+IgD+) in the BM (one femur and one tibia) from *Rev7^{+/+}Mb1^{+/-Cre}* (*n*=8), *Rev7^{F/F}Mb1^{+/-Cre}* (*n*=9), *53bp1^{-/-}Mb1^{+/-Cre}* (*n*=9) mice. *p* values, unpaired two-tailed t-test. Mean ± 95% CI.

(H) Top, schematic of the *Igh* and *Igl* loci and FISH probes. Bottom, representative metaphase images showing normal and abnormal *Igh* and *Igl* loci. C, centromere-proximal; T, telomere-proximal.

(I) *Igh* and *Igl* locus breakage in splenic B cells of indicated mice upon stimulation (anti-CD40 + IL-4) for 96 h. *n*=4 mice per genotype, between 98 and 151 metaphases were analysed from each mouse (*n*=4), except for one WT sample with only 45 metaphases; Multiple comparisons, one-way ANOVA. Mean ± SD.

Figure 2. Mutational screening reveals REV7 interaction surfaces essential for CSR and resection inhibition.

(A) Schematic representation of the screen. *Rev7* single and combinatorial point mutant alleles were stably expressed in *Rev7^{-/-}* CH12-F3. IgM to IgA CSR was measured 40h post stimulation with anti-CD40 antibody, IL-4 and TGFβ-1 (CIT).

(B) Quantification of IgM to IgA CSR in *Rev7^{-/-}* CH12-F3 cell-lines complemented as indicated. IgA switching efficiency normalized against WT REV7 complemented cells. Mutants indicated in

red were excluded from further analysis due to unstable REV7 protein expression. $n=3$ independent experiments. Mean \pm SD.

(C) CSR in stimulated B cells harvested from *Rev7^{F/F}Mb1^{+/-Cre}* mice and infected with GST (control) or indicated *Rev7* mutant-expressing retrovirus. $n=6$ mice per genotype. IgG1-positive events in infected cells as a proportion (%) of the mean IgG1-positive events in 2 WT REV7-complemented controls. Experiments $n=3$ (each 2 mice per genotype). Mean \pm SD.

(D) Representative flow cytometry plots of data in (C).

Figure 3. REV7 interacts with SHLD3 and SHLD1-SHLD2 via distinct surfaces.

(A) B cell REV7 interactome as defined by LC-MS/MS and label-free quantification (LFQ). Scatter plot depict \log_2 fold enrichment of indicated Flag-immunocomplexes across 2 independent experiments.

(B) Interactions between indicated control (AD/BD empty vector), SHLD3, and indicated REV7 proteins by Y2H. 5-fold dilutions, representative data ($n=4$).

(C) Top, schematic of SHLD3, indicating sequence features and positions of alanine substitutions in each mutant protein. Bottom, interactions between REV7 and indicated SHLD3 proteins by Y2H. Representative data ($n=4$).

(D) LC-MS/MS and LFQ analysis of Flag-HA-REV7 and Flag-HA-REV7^{K129A} interactomes. Scatter plot depict \log_2 fold enrichment of interacting proteins across 2 independent experiments.

Figure 4. The REV7-Shieldin complex mediates 53BP1-dependent NHEJ.

(A) Representative flow cytometry plots for IgM to IgA CSR in indicated mutant CH12-F3 cell-lines. Representative data, $n>3$ independent experiments.

(B) IgM to IgA CSR frequencies in knockout CH12-F3 cell-lines. $n=5$ (*Shld3^{-/-}*), $n=4$ (*Shld1^{-/-}*) and $n=3$ (*Shld2^{-/-}*) independent experiments. Mean \pm SD.

(C) IgM to IgA CSR in indicated CH12-F3 lines stably transduced with either control (GST), WT, or mutant SHLD3-expressing transgenes. Data normalized to CSR frequencies of WT CH12-F3. $n=5$ independent experiments. Mean \pm SD.

(D) RPA-ssDNA ChIP with indicated CH12-F3 lines stimulated with CIT (30 h). Representative data, $n=2$ independent experiments. Bars indicate mean.

(E) Clonogenic assay using KB1P-G3 cells following deletion of indicated genes. sgRNA, gene targeted by CRISPR-Cas9 guide RNA.

(F) Quantification of data in (E) and Extended Data Fig. 6k. $n=3$ independent experiments. Mean \pm SD.

(G) Metaphases prepared from indicated cell-lines following 24 h control or olaparib treatment were analysed for the presence of radial chromosomes. $n=3$ independent experiments (each 50 metaphases per condition). Mean \pm SD.

(H) Proposed model of Shieldin-53BP1 cooperation during NHEJ. The stabilization of ssDNA overhangs or ssDNA-dsDNA junctions at DSB sites by REV7-SHLD1-3 complexes promotes DSB resolution activities during NHEJ. The absence of lymphocyte development defects in *Rif1*^{-/-} mice⁹ suggests RIF1 could link 53BP1 anti-resection activities in chromatin to Shieldin activities in ssDNA compartments (arrow).

Table 1. Label Free Quantification (LFQ) of LC-MS/MS results for indicated interacting proteins as determined in Fig. 3a, d. ND, not determined. *n*=2 independent experiments.

Methods

Mice

All mice used for this study were generated on, or backcrossed onto a C57BL/6 background (>10 generations). Sperm from mice harbouring the *Mad2l2*^{tm1a(EUCOMM)Wtsi} knockout-first conditional allele for *Rev7* (MGI:4432091, a gift from David Adams, Wellcome Sanger Institute, Hinxton, UK), was used to re-derive *Mad2l2*^{tm1a(EUCOMM)Wtsi/+} mice, which were then bred with constitutive *Flp*-deleter mice (Tg(*ACTB-Flpe*)9205Dym; Jax stock 005703) to generate mice with the *Mad2l2*^{tm1c} conditional allele. Experimental *Rev7*^{F/F} *Mb1*^{+/-cre} (*Mad2l2*^{tm1c/tm1c}) and related control mice were generated by intercrossing with mice harbouring the B cell lineage *Mb1-cre* deleter strain (*Cd79a*^{tm1(cre)Reth}; MGI:3687451¹⁴). All experiments involved age-matched 8-16 week-old animals on an inbred C57BL/6 background. *53bp1*^{-/-} mice (MGI:2654201; also C57BL/6) were generated and described elsewhere²⁸. For bone marrow mixed chimera experiments, wild-type C57BL/6-Ly5.1 mice (hereafter known as CD45.1; Jax stock 002014) were irradiated with two doses of 4.5 Gy spaced 3 h apart, and subsequently injected with 5-10 x 10⁶ bone marrow cells (approximately 50:50 mixture) of wt CD45.1⁺ bone marrow and either wt *Mb1*^{+/-Cre}, *Rev7*^{F/F} *Mb1*^{+/-Cre} or *53bp1*^{-/-} *Mb1*^{+/-Cre} (CD45.2⁺) bone marrow. Baytril 10 % antibiotic solution (Vet Services, University of Oxford) was added to drinking water (1.5 mL to 250 mL water) for 3 weeks after irradiation. Mice were allowed to reconstitute for 7-8 weeks before analysis. Sample sizes were determined by power calculations. We were not pursuing lower penetrance phenotypes, thus statistically significant data could typically be obtained with small group sizes (typically, 4-10 mice). Randomization of samples was only undertaken during the scoring of chromosomal aberration during metaphase analyses. Mice of a certain genotype were selected based on a unique mouse ID# that does not indicate mouse genotype, thus phenotype-genotype relationships were determined only at the data analysis stage. All experiments were approved by the University of Oxford Ethical Review Committee and performed under a UK Home Office Licence in compliance with animal use guidelines and ethical regulations.

Immunizations

Mb1^{+/-Cre}, *Rev7*^{F/F} *Mb1*^{+/-Cre}, or *Rev7*^{F/F} *Mb1*^{+/-Cre} mice were immunized intraperitoneally with 50 mg of NP-CGG (Santa Cruz Biotechnologies) emulsified in Imject Alum adjuvant (Pierce, Thermo Fisher Scientific). Blood samples were collected from the tail vein at 0, 7, 14, 21 and 28 days after immunization.

ELISA

Enzyme-linked immunosorbent assays (ELISAs) were used to quantify the production of NP-specific antibodies in mice serum. 96 well plates were coated with 1 µg/ml NP-BSA (Biosearch Technologies) in bicarbonate buffer, blocked with 5% milk in PBS and incubated with serial

dilutions of serum collected at different time points from immunized mice. Plates were probed using alkaline phosphatase-coupled antibodies against mouse IgM and IgG1 (Southern Biotech). Phosphatase substrate (Sigma) was used for detection and optical density measured at 405nm. For IgG1, pooled blood from post-immunisation wild type mice was used as a standard and serially diluted into a standard curve. The first dilution was established as 1000 arbitrary units. For IgM pooled blood from day 7 was used as a standard. Ig concentrations in mouse serum or culture supernatants were determined by sandwich ELISA. Total IgG, IgM and IgA was measured with mouse IgG, IgM and IgA ELISA kits, respectively (Bethyl Laboratories), according to the manufacturers instructions. Mouse serum with known Ig concentrations of each Ig was used as a standard.

B-lymphocyte analysis and flow cytometry

Cell suspensions from bone marrow (one femur and one tibia) and spleen were counted on a haemocytometer and stained with anti-mouse antibodies against the following antigens as appropriate (all from BioLegend unless otherwise stated) in FACS buffer (PBS with 2% BSA and 0.025% sodium azide): IgD (1:500, 405716 or Thermo Fisher 12-5993-82; 11-26c.2a), IgG1 (1:200, 406606; RMG1-1), IgM (1:500, 406506 or 406514; RMM-1), B220 (1:500, 103232, 103244, 103206, or 103212; RA3-6B2), BP-1 (1:200, 108308; 6C3), CD19 (1:500, 115534 or 115520; 6D5), CD24 (1:1000, 101827 or BD Pharmingen 562563; M1/69), CD93 (1:200, 136510; AA4.1), CD23 (1:200, BD Pharmingen 553139; B3B4), CD43 (1:200, BD Pharmingen 562865; S7, or Thermo Fisher 11-0431-85; eBioR2/60), and CD21 (1:500, BD Biosciences 563176; 7G6). Mouse BD Fc Block (1:500, BD Pharmingen 553141) was added to block non-specific binding and live/dead cells were discriminated after staining with Zombie Aqua viability dye (1:200, 423102) or Zombie NIR viability dye (1:500, 423105). Bone marrow cells from mixed chimeras were also stained against CD45.1 (1:500, 110730; A20) and CD45.2 (1:500, 109818; 104). Data were acquired on a FACSCanto (BD Biosciences), SH800 (Sony), or MoFlo Legacy (Beckman Coulter) and were analyzed with FlowJo Software v10 (Tree Star). Gating strategies for bone marrow (left panel) and spleen (right panel) are shown in Supplementary Figure 2; further Hardy Fraction gating strategies are shown in Extended Figure 2a.

Ex vivo B splenocyte culture, stimulation and flow cytometry

B cells were purified from red blood cell-lysed single-cell suspensions of mouse spleens by magnetic negative selection using a B Cell Isolation Kit (Miltenyi Biotec, 130-090-862). B cells (3×10^5 per well in a 12-well plate) were cultured in RPMI supplemented with 10% FCS, 100 U/ml penicillin, 100 ng/ml streptomycin, 2 mM L-glutamine, 1x MEM nonessential amino acids, 1 mM sodium pyruvate and 50 μ M β -mercaptoethanol. B cells were stimulated with 5 μ g/ml LPS (Sigma, L7770-1MG), 10 ng/ml mouse recombinant IL-4 (Peprotech, 214-14-20), and agonist

anti-CD40 antibody (0.5 µg/ml; Miltenyi Biotec; FGK45.5). Cultures were grown at 37°C with 5% CO₂ under ambient oxygen conditions. Four days after seeding, stimulated B cells were analysed using a FACSCanto; analysis was performed using FlowJo. Cells were resuspended in FACS buffer, blocked with Mouse BD Fc Block, and immunostained with biotinylated antibodies as follows: anti-mouse IgG1 (1:100, BD Pharmingen 553441; A85-1), anti-mouse IgG2b (1:100, BioLegend 406704; RMG2b-1), anti-mouse IgG3 (1:100, BD Pharmingen 553401; R40-82) and Streptavidin APC (1:500, Thermo Fisher 17-4317-82). Cells expressing IgE were assessed using anti-Mouse IgE PE (BioLegend, 406908; RME-1). Live/dead cells were discriminated after staining with Zombie Aqua viability dye. Cell proliferation was assessed using Cell Trace Violet according to manufacturer's instructions (CellTrace, Life Technologies).

Primary B cell reconstitution

Mature untouched B cells were purified as above and stimulated with LPS (5 µg/ml, Sigma, L7770) and mouse recombinant IL-4 (10 ng/ml, Peprotech, 214-14-20). Cultures were grown at 37°C with 5% CO₂ under ambient oxygen conditions. Filtered retroviral supernatants harvested 48 h following co-transfection of BOSC23 cells with 7 µg pCL-Eco and 7 µg pMX-IRES-GFP-derived plasmids were used to infect LPS/IL-4-stimulated B cell cultures the presence of polybrene (2.5 µg/ml) and HEPES (20 mM) by spinoculation (850 x g for 90 min at 30°C). After a rest period of 4 to 6 hours, viral supernatants were removed, and replaced with LPS/IL-4-supplemented culture medium. Three days later, surface IgG1 expression was determined in gated cells populations positive for the expression of an eGFP retroviral reporter.

CH12-F3 cell culture and CRISPR-Cas9 editing

All CH12-F3 cell lines were cultured in RPMI supplemented with 5 % NCTC-109 medium, 10% FCS, 100 U/ml penicillin, 100 ng/ml streptomycin and 2 mM L-glutamine at 37°C with 5% CO₂ under ambient oxygen conditions. *REV7^{-/-}*, *c20orf196^{-/-}* (*SHLD1^{-/-}*), *FAM35A* (*SHLD2^{-/-}*) and *FLJ26957* (*SHLD3^{-/-}*) CH12-F3 were generated using CRISPR-Cas9. Briefly, gene-specific sgRNAs (sgRNA sequences in Extended Data Table 3a) were cloned in modified pX330 (Addgene #42230) or pX458 vectors (Addgene #48138). CH12-F3 cells were nucleofected (Amaza Nucleofector 2b, Lonza) with 2 µg of plasmid and Cell Line Nucleofector Kit R (Lonza), using program D-023. Isogenic cell clones were isolated by limiting dilution (pX330) or GFP sorting (pX458) single cell into 96 well plates. Clones bearing bi-allelic indel mutations were identified by native PAGE resolution of PCR amplicons corresponding to edited loci (Amplicon primer sequences in Extended Data Table 4a), and gene disruption subsequently confirmed by Sanger sequencing (sequencing results in Extended Data Table 3b). Where antibodies were available, effective target protein ablation was confirmed by immunoblotting. Complemented cell lines were generated by lentivirus-mediated transduction, using viral supernatants harvested from 293T cells co-transfected with third generation packaging vectors and pLenti-PGK-PURO-

DEST (Addgene #19068) or pLenti-PGK-Flag-HA-PURO-DEST vectors containing cloned transgene inserts. Typically, cells were spinoculated with polybrene (8 µg/ml) and Hepes (20 mM)-supplemented viral supernatants (1500 rpm, 90 min at 25°C). Stable cell-lines were subsequently selected and maintained in the presence of puromycin (1 µg/ml). To stimulate CSR to IgA, CH12-F3 cells were stimulated with agonist anti-CD40 antibody (0.5 µg/ml; Miltenyi Biotec; FGK45.5), mouse IL-4 (5 ng/µl; R&D Systems) and TGF-β1 (2.5 ng/µl; R&D Systems). Cell-surface IgA expression was determined by flow cytometric staining with anti-mouse IgA-FITC antibody (Thermo Fisher; 11-4204-82; MA-6E1). CH12-F3 proliferation was monitored by dye dilution using carboxyfluorescein succinimidyl ester (CFSE) according to manufacturer's instructions (CellTrace; Life Technologies). In cell cycle experiments, CH12-F3 pulse-treated with BrdU for 30 min before fixation in 70% ethanol, were stained with propidium iodide and rat anti-BrdU-FITC (1:100, Bio-Rad MCA2060FT). Certified mycoplasma free CH12-F3 were obtained by Cell Services (Francis Crick Institute, London, UK). These and other cell-lines (e.g. 293T, BOSC-23) were confirmed free of mycoplasma contamination.

Antibodies

Immunoblot primary antibodies used in this study; α-Rif1: Clone SK1316; gift of Ian Adams²⁹; α-Histone H3: Abcam ab10799, clone 10799; 1:2000; α-Rev7: BD 612266, clone 14/MAD2B/Rev7, 1:500; α-53BP1: Novus Biologicals NB100-304, 1:2500; α-HA-11: BioLegend 901501, Clone 16B12, 1:2000; α-Actin: Sigma A1978, Clone AC15, 1:2000; α-tubulin: Sigma 00020911, Clone TAT-1, 1:10000. Proteins were detected using HRP-conjugated secondary antibodies (α-rabbit, Thermo Fisher 31462, 1:50,000; α-mouse, Thermo Fisher 31432, 1:50,000; Mouse TrueBlot ULTRA, Rockland 18-8817-33, 1:5000) and enhanced chemiluminescence (Clarity, Bio-Rad). Signals were acquired digitally on a Gel Doc™ XR system (Bio-Rad).

Proteomics and mass spectrometry

Pellets harvested from cultures of ~4x10⁷ CH12-F3 were lysed in BLB (Benzonase Lysis buffer: 20 mM HEPES pH 7.9, 40 mM KCl, 2 mM MgCl₂, 10% glycerol, 0.5% NP40, 50 U/ml Benzonase (Novagen), 0.05% (v/v) phosphatase inhibitors (Sigma-Aldrich) and protease inhibitors (Complete EDTA-free, Roche)) and were incubated on ice for 30 min before a second incubation with adjusted salt (450mM KCl). Flag-REV7 or control complexes were isolated from clarified lysates, following their dilution in NSB (no-salt buffer: 20 mM HEPES (pH 7.9), 10% Glycerol, 0.5mM DTT, 0.5 mM EDTA, 0.05% [v/v] phosphatase inhibitors [Sigma-Aldrich] and protease inhibitors [Roche]) to a final salt concentration of 125 mM. Flag-HA-REV7 complexes were immunopurified on anti-FLAG(M2) magnetic resin (Sigma-Aldrich), washed extensively in wash buffer (BLM supplemented with 125 mM KCl and 0.1% NP-40) and eluted with 3× Flag peptide (Sigma-Aldrich). Flag-peptide eluted complexes were reduced and alkylated using DTT and iodoacetamide, followed by a Chloroform/Methanol precipitation. Proteins were resuspended in

6M Urea and digested over night with trypsin (Promega). Peptides were desalted (Sola, Thermo) analysed on a LC-MS platform consisting of a Dionex Ultimate 3000 nHPLC and Q-Exactive mass spectrometer. Peptides were separated on an EASY-Spray column (50 cm, ES803, Thermo) with a gradient of 3-35% Acetonitrile in 5% DMSO and 0.1% formic acid @ 250 nl/min. MS1 spectra were acquired at a resolution of 70000 @ 200m/z. Up to the 15 most abundant precursor ions were selected for subsequent MS/MS analysis after ion isolation with a mass window of 1.6 Th. Peptides were fragmented by HCD with 28% collision energy. Progenesis QI (v. 3, Waters) was used for spectral counting and LFQ of the LC-MS/MS data with default parameters (Top 3 quantitation mode). Proteins were identified with PEAKS 8.0 (Bioinformatics Solutions) using standard parameters and the Uniprot mouse reviewed proteome (retrieved 28/11/2017). Peptide false discovery rate was set to 1% with a resulting protein FDR of 1.88%.

Chromatin Immunoprecipitation

Each ChIP was performed from chromatin prepared from $\sim 10^7$ CH12-F3 cells stimulated for 30 h with agonist CD40 antibody, IL-4, and TGF- β as previously described¹³. Each ChIP was performed using 30–50 μ g CH12-F3 chromatin using RPA34-20 (3 μ g; Ab-3, Calbiochem) or Anti-Histone H3 (2 μ g; ab1791, Abcam) coupled to 25 μ l Protein-G Dynabeads® (Life Technologies, 10003D). Relative quantities of ChIP-enriched DNA were calculated relative to total input chromatin by qPCR in triplicate on CFX96 Real-Time Analyzer (Bio-Rad) or StepOnePlus (Applied Biosystems) instruments using Quantifast SYBR Green reagent (QIAGEN) and locus-specific primer pairs (Extended Data Table 4b).

Yeast two-hybrid (Y2H) interaction

Open reading frames encoding the indicated proteins were cloned into pAD-DEST and pBD-DEST vectors and transformed into *S cerevisiae* (strain PJ69-4A). 10 ml cultures prepared from single transformants were diluted to equal volumes containing 2×10^7 cells, and 5-fold serial dilutions “spotted” on control (-Leu -Trp) or experimental (-Leu -Trp -His) plates supplemented with 3-Amino-1,2,4-triazole (3-AT, 6 mM, Sigma A8056). Plates were incubated at 30°C for 3 days.

PARPi resistance

KB1P-G3 and *53Bp1*^{-/-} KB1P-G3 cells were infected with viral supernatant generated using lentiCRISPR-Bsr. Following selection in blasticidin (10 mg/ml), genomic DNA (gDNA) samples were collected immediately prior to seeding for olaparib sensitivity. Blasticidin-resistant populations were seeded in 6-well plates at a density of 10^4 cells per well (5×10^3 for *53Bp1*^{-/-} KB1P-G3) in the presence of olaparib or DMSO and grown at 37°C (5% CO₂ and 3% O₂). Medium was refreshed at 4 days and 8 days. After 10 days, cultures were expanded in fresh medium for 1 week in 6 cm dishes before harvesting gDNA. PCR amplicon encompassing the

edited locus were PCR amplified from gDNA, sanger sequenced (GATC Biotech), and analysed by Tracking of Indels by Decomposition (TIDE: <https://tide.deskgen.com/>). Surviving cells were collected and three replicates were plated in DMSO and three in olaparib for viability analysis. DMSO and olaparib-treated cells were stained with crystal violet (0.5% (w/v) crystal violet in 25% methanol) after 8 days and 10 days growth (37°C, 5% CO₂ and 3% O₂), respectively. Crystal violet stained cells were dissolved in a 10% (v/v) acetic acid solution a minimum of 24 h after staining and the OD₅₉₅ was measured as a quantitative metric of relative growth. In Fig 5g, cells were incubated for 24 hours in Olaparib 250 nM in standard medium, before metaphase chromosomes were harvested.

Cytological analysis

Metaphase spreads were prepared by standard methods. Briefly, detached cells were resuspended in KCl 75 mM for 20 minutes, before being fixed in Carnoy's fixative. Approximately 20 µl of cell suspension was dropped onto clean slides and left to dry overnight. The cells were then stained with propidium iodide 0.5µg/ml in PBS for 20 minutes, rinsed and the slides mounted in Vectashield/DAPI (Vector Labs). The slides were analysed blind, and a minimum of 50 metaphases were acquired using an Olympus BX60 microscope for epifluorescence equipped with a Sensys CCD camera (Photometrics, USA). Images were collected using Genus Cytovision software (Leica).

FISH analysis

BAC probes (RP23-41J14 (*Igh* 3'); RP24-316H6 (*Igh* 5') (gifts from the Wellcome Sanger Institute, Hinxton, UK); RP23-374P12 (*Igl* 3'); RP23-382P9 (*Igl* 5') (Source Bioscience) were labelled using a nick translation kit (Abbott Molecular) according to the manufacturer instructions, incorporating either Chromatide Alexa Fluor 594-5-dUTP (Thermo Fisher Scientific), Chromatide Alexa Fluor 488-5-dUTP (Thermo Fisher Scientific), Gold-dUTP (Abbott Molecular) or biotin-16-dUTP (Sigma). The probes were resuspended in the presence of a ten times excess of unlabelled mouse C0t1 DNA (Thermo Fisher Scientific), in hybridization buffer (50% formamide, 10% dextran sulphate, 2xSSC), before being denatured for 8 minutes at 85°C, followed by a pre-annealing step 30 minutes at 37°C. The metaphase spreads were denatured in 0.07 N NaOH for 1 minute. The probes were applied onto the slides, and the hybridization was carried out overnight at 37°C. Three post-hybridization washes were performed, in 0.1x SSC buffer at 65°C. Biotinylated probes were detected using streptavidin-Cy5 (Thermo Fisher Scientific). Slides were mounted in Vectashield/DAPI and analysed blind with the microscope described above. Between 98 and 150 metaphases were analysed for each mouse with the exception of one case (45 metaphases collected for 1 control mouse).

Additional References

28. Ward, I. M., Minn, K., van Deursen, J. & Chen, J. p53 Binding protein 53BP1 is required for DNA damage responses and tumor suppression in mice. *Mol. Cell. Biol.* **23**, 2556–2563 (2003).
29. Adams, I. R. & McLaren, A. Identification and characterisation of mRif1: a mouse telomere-associated protein highly expressed in germ cells and embryo-derived pluripotent stem cells. *Dev Dyn* **229**, 733–744 (2004).
30. Skarnes, W. C. *et al.* A conditional knockout resource for the genome-wide study of mouse gene function. *Nature* **474**, 337–342 (2011).
31. Khalaj, M. *et al.* A missense mutation in Rev7 disrupts formation of Polζ, impairing mouse development and repair of genotoxic agent-induced DNA lesions. *Journal of Biological Chemistry* **289**, 3811–3824 (2014).
32. Kikuchi, S., Hara, K., Shimizu, T., Sato, M. & Hashimoto, H. Structural basis of recruitment of DNA polymerase ζ by interaction between REV1 and REV7 proteins. *Journal of Biological Chemistry* **287**, 33847–33852 (2012).
33. Wagner, S. A. *et al.* A proteome-wide, quantitative survey of in vivo ubiquitylation sites reveals widespread regulatory roles. *Molecular & Cellular Proteomics* **10**, M111.013284 (2011).

Extended Data Figure Legends

Extended Data Figure 1. CSR characterisation in *Rev7* conditional-knockout mice

(A) PCR amplicons from genomic DNA obtained by ear biopsies or purified splenic B cells (left panel), or flow cytometry sorted cells from Hardy Fractions A, B, and C (right panel) from mice with the indicated genotype. Bands of different size correspond to the *Rev7^{tm1c}* allele (Cond=475bp), *Rev7⁺* allele (WT=314bp) and *Rev7^{tm1d}* allele (Flox= 255bp). Representative data; *n*>3 experiments.

(B) Western blot analysis of REV7 protein expression in splenic B cell isolated from mice with the indicated genotype. Representative data; *n*=2 experiments. For gel source data, see Supplementary Figure 1.

(C) CTV-labelled purified B cells were stimulated as indicated and stained for surface IgG1 (left panel) or IgG2b (centre panel) or IgG3 (right panel) on day 4. Representative of *n*>6 experiments.

Extended Data Figure 2. B cell lineage developmental differences in *Rev7*- and *53bp1*-deficient mice.

(A) Flow cytometry analysis of B cell development in the bone marrow (BM) of *Rev7^{+/+}Mb1^{+/Cre}*, *Rev7^{F/F}Mb1^{+/Cre}*, and *53bp1^{-/-}Mb1^{+/Cre}* mice; gating on B220⁺CD43⁺ (left panels, Hardy Fractions

A-B-C) and on B220⁺CD43⁻ (right panels, Hardy Fractions D-E-F). Representative data; $n > 8$ experiments.

(B) Apoptotic indices of total, pro/pre-, immature, and mature B cell fractions in the BM (left panel) and spleen (right panel) of *Rev7^{+/+} Mb1^{+/-Cre}* ($n=4$), *Rev7^{F/F} Mb1^{+/-Cre}* ($n=4$), *53bp1^{-/-} Mb1^{+/-Cre}* ($n=2$) mice.

(C) Flow cytometric sub-classification of mature splenic B cell fractions in *Rev7^{+/+} Mb1^{+/-Cre}* ($n=8$), *Rev7^{F/F} Mb1^{+/-Cre}* ($n=8$), *53bp1^{-/-} Mb1^{+/-Cre}* ($n=9$) mice. p -values, unpaired Students two-tailed t-test. Bars represent mean \pm 95% CI.

(D) Top panel: Indicated populations of pooled Pro- to Pre- B cell stage BM lymphocytes (B220⁺CD43⁺; Hardy Fr. A-B-C) from $n=2$ mice per genotype were FACS sorted and used to generate whole cell extracts. Bottom panel: Immunoblot shows an absence of REV7 protein in extracts prepared from *Rev7^{F/F} Mb1^{+/-Cre}* experimental BM, when compared to extracts prepared from *Rev7^{F/F} Mb1^{+/+}* (no Cre) controls, yet equivalent levels of 53BP1, Histone H3 (loading control), and total protein (Ponceau S stain). For gel source data, see Supplementary Figure 1.

(E) Left panel: Diagram of the mixed bone marrow chimera transplantation experiment. Bone marrow cells from a wild-type CD45.1⁺ donor mouse were combined with an equal number of bone marrow cells from an experimental CD45.2⁺ donor mouse, and injected into lethally irradiated recipient CD45.1⁺ mice ($n=8$ per genotype). After 8 weeks, the recipient bone marrow was analysed for the relative contribution of CD45.1⁺ or CD45.2⁺ cells to reconstitute the recipient mice. Right top panels: Enumeration of B cell precursors (as per Fig. 1g) of CD45.1⁺ (white circles) or CD45.2⁺ (from *Rev7^{F/F} Mb1^{+/-Cre}*, or *53bp1^{-/-} Mb1^{+/-Cre}* mice; black circles) cells in the bone marrow following reconstitution. Right bottom panel: stage-specific ratios of CD45.1⁺ to CD45.2⁺ grafted B cells for indicated mixed chimeras. In parallel, an additional control experiment involving wild type CD45.1 and *Mb1^{+/-Cre}* mixed chimera was performed, resulting in equal CD45.1:CD45.2 reconstitution (data not shown). p -values, Multiple t-test with Holm-Sidak correction; Mean \pm 95% CI.

Extended Data Figure 3. REV7 protein expression and CSR in complemented *Rev7^{-/-}* CH12-F3.

(A) Stable Flag-HA-REV7 protein expression in indicated complemented CH12-F3 cell-lines as determined by western blotting with HA-specific antibody. Tubulin serves as loading control. Representative data; $n > 3$ independent experiments. For gel source data, see Supplementary Figure 1.

(B) Flow-cytometric plots of CSR data in Fig. b. Representative data; $n > 3$ independent experiments.

(C) Chromatin prepared from indicated CH12-F3 lines 30 h following stimulation, was subjected to ChIP with RPA34 or histone H3 (control) antibodies. Schematic, mouse *Igh* locus with

positions of qPCR amplicons. ChIP recoveries were quantified against input DNA. Representative data, $n=2$ independent experiments. Mean \pm SD.

Extended Data Figure 4. Distinct REV7 residues mediate its functions in ICL repair.

(A) Indicated REV7 mutants were tested for their interaction with the REV3L RBM₁ by yeast-2-hybrid. A fragment of REVL3 (aa¹⁷⁷⁵⁻²²⁰⁰) with RBM₂ mutated (P1996A, P2001A). 5-fold dilutions, $n=4$ biological repeats.

(B) Representative histograms of indicated CH12-F3 lines, mock or MMC treated for 8 and 24 h. Numbers depict sub-G1 and G2/M populations as a proportion (%) of total events. Representative data, $n=3$ independent experiments.

(C) Representative PI/DAPI stained metaphases from indicated CH12-F3 cell-lines following 24 h incubation with MMC; $n=2$ independent experiments.

(D) Blind quantification of DSBs (chromatid and chromosome-type) and radials in indicated cell lines, with each metaphase scored as a single point. $n=2$ independent experiments, each with 50 metaphases scored per genotype and condition. Bars indicate mean.

(E) Cell cycle of indicated CH12-F3 lines following MMC treatment. Proportions (%) of sub-G1, G1, S, and G2/M events. $n=3$ independent experiments \pm SD.

Extended Data Figure 5. Identification of the REV7-Shieldin complex.

(A) N-terminal SHLD3/FLJ26957 sequences contain conserved REV7-binding motifs (RBM₁ and RBM₂). Pairwise alignment of REV3L RBM1 with SHLD3 RBM₁ and RBM₂ across multiple species. Black and grey shading indicate identical and similar residues, respectively.

(B) Surface representation of REV7 crystal structure (RCSB pdb: 4FJO), pseudo-coloured according to amino-acid conservation. V, variable, and C, conserved residues.

(C) Protein threading model of FAM35A identifies an RPA70-like triple OB-fold architecture. The FAM35A structural model generated using Phyre2 predicts amino acid residues 429-826 (coloured in green) adopt the same folds as *Ustilago maydis* RPA70 (pdb: 4GOP, chain C; 99.5% confidence in the model²⁴). Blue structural chains from RPA70 are inserted in regions of FAM35A that could not be modelled with high confidence (internal and FAM35A residues 826+). In the Shieldin complex, RPA34 (opaque red) and RPA14 (opaque yellow) subunits of the heterotrimeric RPA complex might be substituted with SHLD1, SHL3 and REV7 proteins.

(D) Pairwise alignment shows 16% sequence identity across human FAM35A isoform 2 (OB-folds 1-3) and *Ustilago maydis* RPA70 (OB-folds 2-4; generated with Phyre2). Black and grey shading indicate identical and similar residues, respectively.

Extended Data Figure 6. SHLD3 (FLJ26957) mediates 53BP1-dependent NHEJ.

(A) Immunoblot showing levels of REV7, 53BP1, and REV7 protein in whole cell lysates prepared from indicated CH12-F3 cell lines. Representative of $n=2$ individual experiments. For gel source data, see Supplementary Figure 1.

(B) Normal proliferation of stimulated wild type and *Shld3*^{-/-}, *Shld1*^{-/-} and *Shld2*^{-/-} CH12-F3. CFSE dye dilution assay. $n=2$ independent experiments.

(C) Summary of IgM to IgA CSR frequencies in indicated control GST or HA-SHLD2(mouse) - complemented *Shld2*^{-/-} CH12-F3. Data normalized to CSR in WT cells. $n=4$ independent experiments; mean \pm SD.

(D) IgM to IgA CSR in indicated CH12-F3 *Shld3*^{-/-} \pm complementation with wild-type SHLD3 or SHLD3^{P53A-P58A} (RBM2 mutated). Data normalized to CSR in WT cells. Mean \pm SD ($n=4$).

(E) Summary of IgM to IgA CSR frequencies in *Rev7*^{-/-} and *Rev7*^{-/-} *Shld3*^{-/-} double knockout CH12-F3 clones. Data normalized to CSR in WT cells. $n=4$ independent experiments; mean \pm SD.

(F) Histone H3 (control) ChIP efficiencies at indicated *Igh* and control loci. Related to RPA-ChIP data in Fig. 4d. Representative data, $n=2$ independent experiments. Mean \pm SD, 2-3 qPCR replicates.

(G) Indicated CH12-F3 lines stimulated with CIT (30 h) were subjected to ChIP experiments with RPA34 and histone H3 (control) antibodies. Representative data, $n=2$ independent experiments. Mean \pm SD, 2-3 qPCR replicates.

(H) Cell cycle of indicated CH12-F3 lines following MMC treatment. Proportions (%) of sub-G1, G1, S and G2/M events. $n=3$ independent experiments; mean \pm SD.

(I) Change (%) of Cas9-dependent indels at the indicated sgRNA locus in KB1P-G3 cells after outgrowth in DMSO or Olaparib (300 nM) for 7 days. Representative data, 2 independent experiments.

(J) As in Extended Data Fig. 6i but with *53bp1*^{-/-} KB1P-G3. Representative data, $n=2$ independent experiments.

(K) As in Fig. 4e but with *53bp1*^{-/-} KB1P-G3. Representative data, $n=3$ independent experiments.

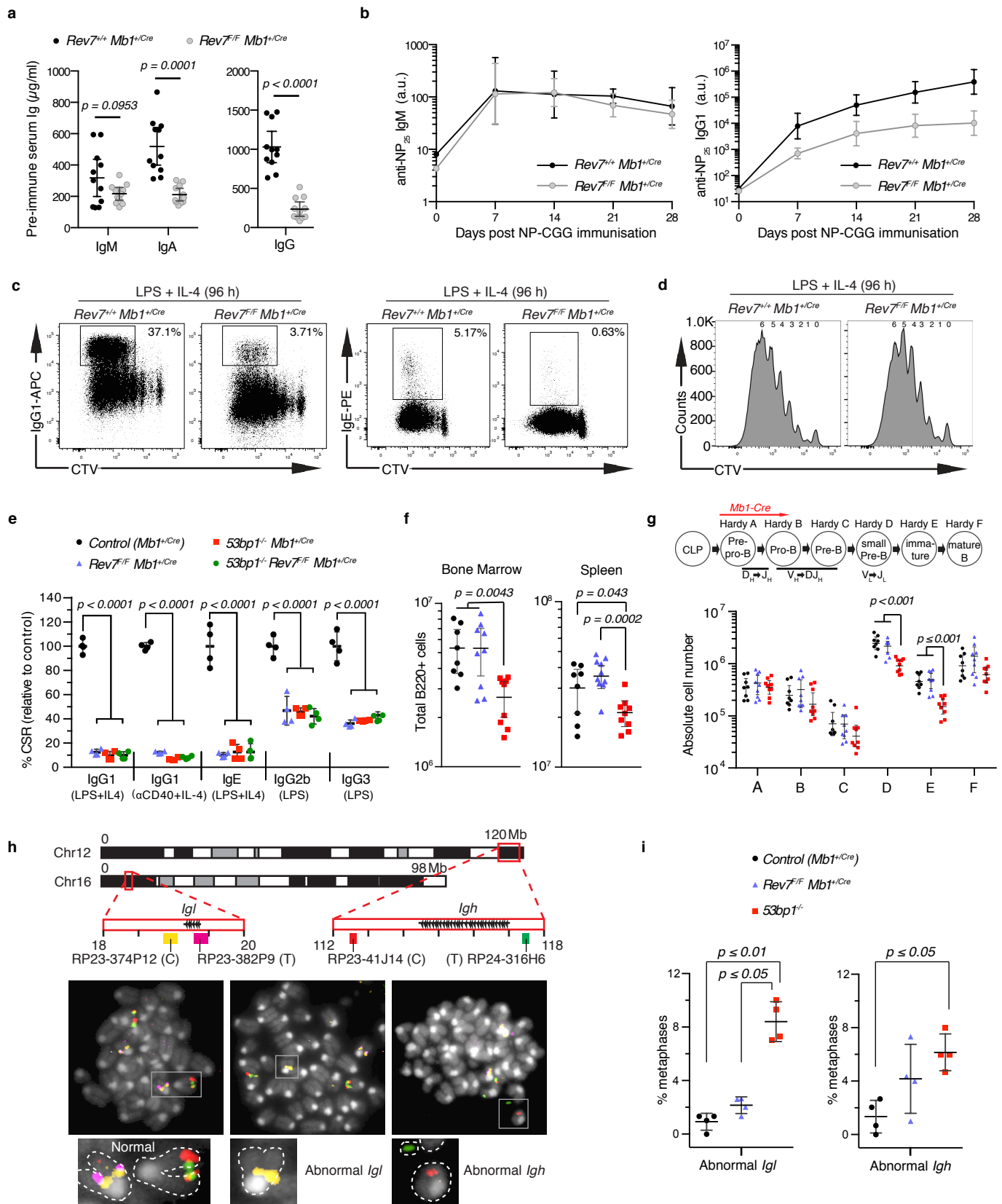
Extended Data Table 1. Predicted and observed offspring of *Rev7* mutant mice (*Rev7*^{tm1a(EUCOMM)Wtsi}, MGI:4432091) bred in this study on a C57Bl/6 background. IMPC, International Mouse Phenotyping Consortium.

Extended Data Table 2. Mutant mouse REV7 proteins generated and phenotyped in this study.

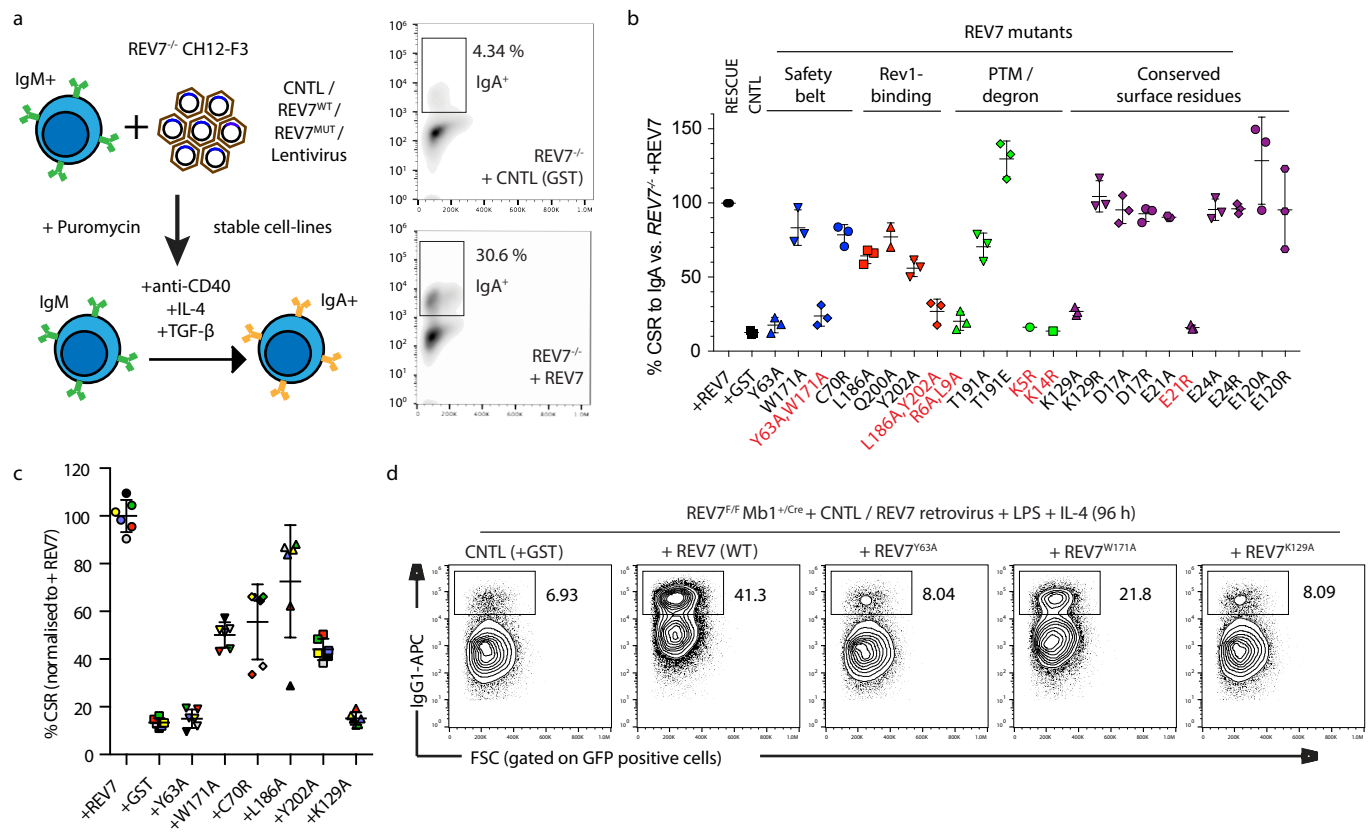
Extended Data Table 3. CRISPR-Cas9 reagents and edited cell-lines generated in this study. (A) Sequences of sgRNA used in gene editing experiments. S, indicates sgRNA

corresponds to sense strand; AS, indicates antisense strand. (B) Individual edited alleles in each cell-line clone as confirmed by Sanger sequencing.

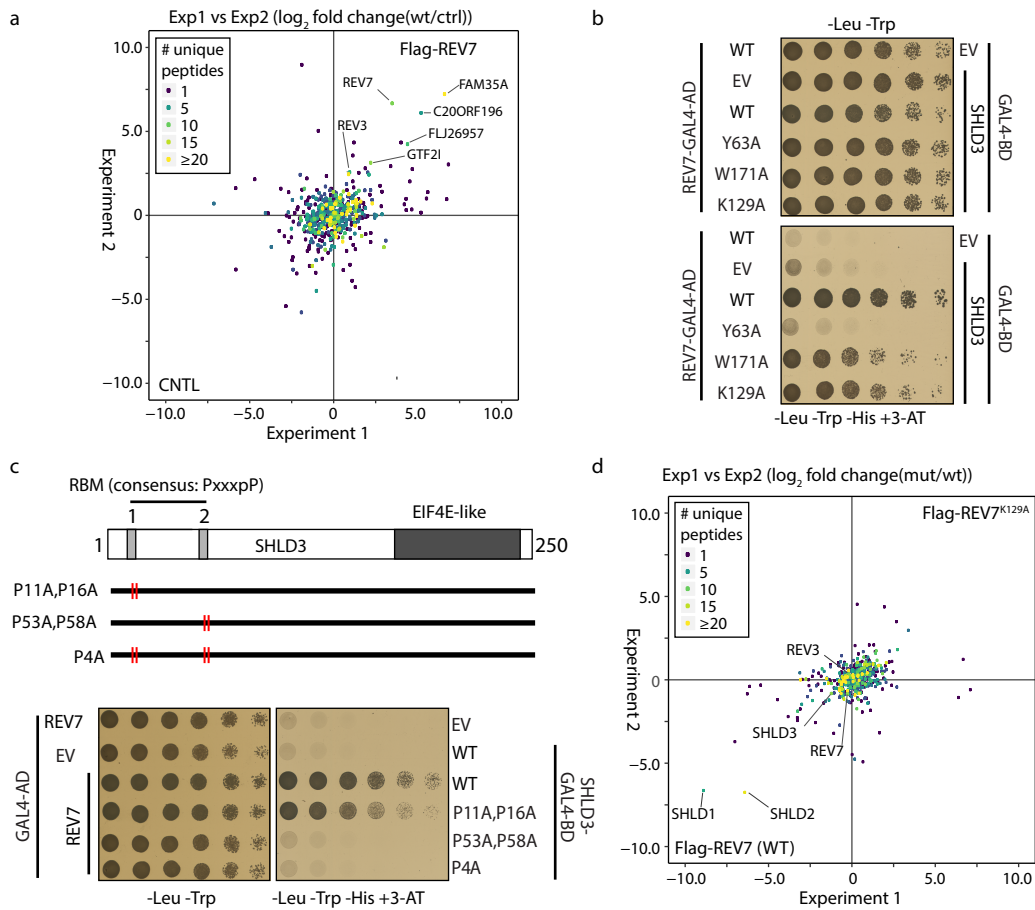
Extended Data Table 4. Primers used in this study. (A) Primers used to amplify CRISPR-Cas9 target loci in edited cell-lines. (B) Locus-specific ChIP amplicon qPCR primer sequences.

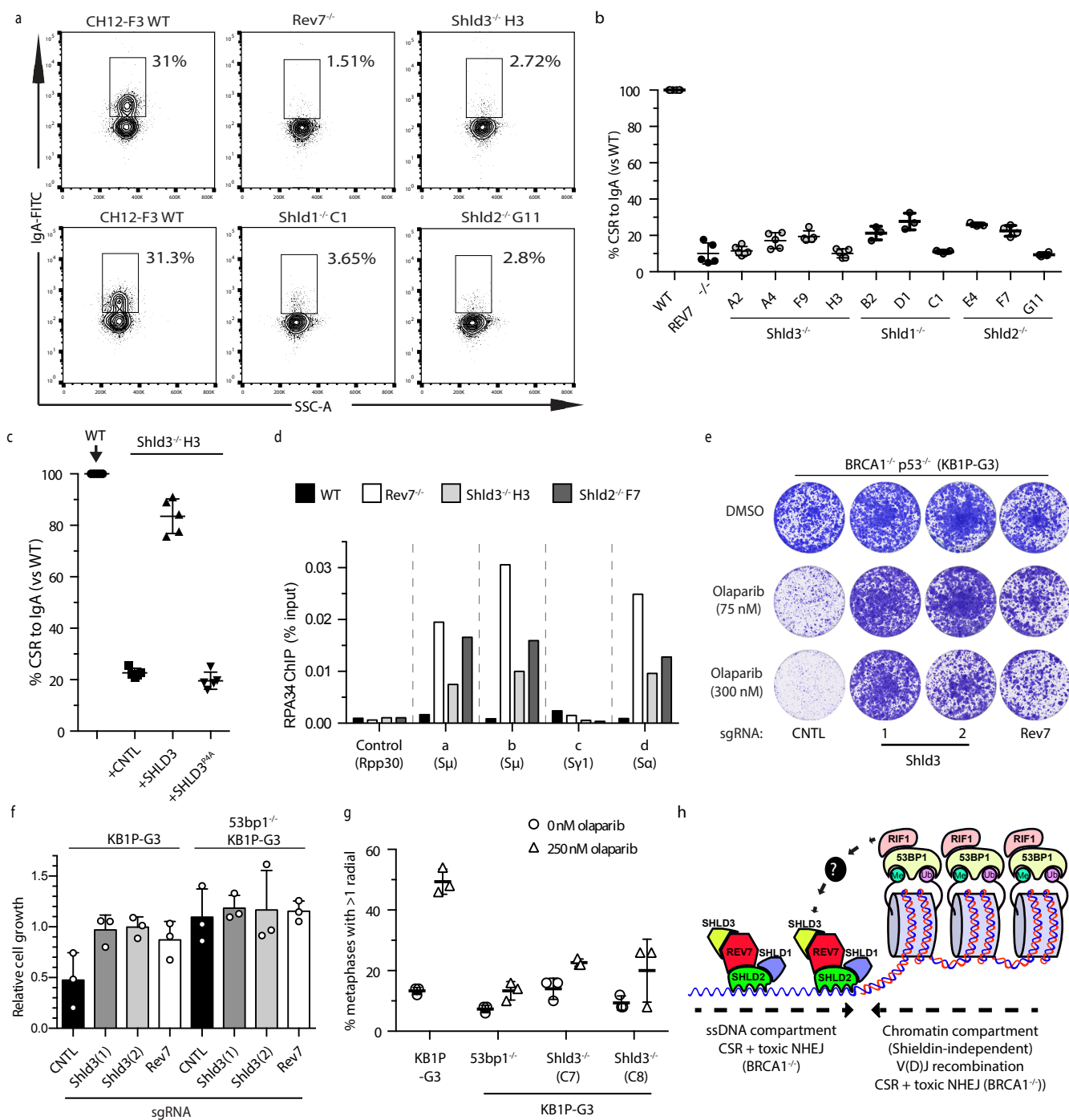


Ghezraoui et al. Figure 1



Ghezraoui et al. Figure 2





Ghezraoui et al. Figure 4